Geoacoustical Parameters Estimation With Impulsive and Boat-Noise Sources

Barbara Nicolas, Jérome Mars, and Jean-Louis Lacoume, *Senior Member, IEEE*

***Abstract*—Localization is a crucial issue in underwater acoustics: when an underwater source is detected, the next step consists of localizing it. To do this, environmental parameters must be known or estimated. How can we estimate these parameters? As underwater sources produce low frequency (<100 Hz), most of the seismic processing tools developed by petroleum research can be adapted to estimate geophysical parameters of the sea and the seafloor. To know which methods or representations are useful to estimate geoacoustical parameters, a study of the propagation between an underwater source and receivers laid on the floor is proposed in the case of a real waveguide. Then, geoacoustical parameters are estimated on real data using transformations such as velocity correction or frequency-wavenumber transform. To validate these methods, two wave-propagation simulations using a finite-difference algorithm are made: the first in an environment similar to the model used to estimate geoacoustical parameters and the second in a more realistic environment (with several layers of sediments and variable water layer depth). Geoacoustical parameters are estimated and compared to the values used in the simulation. Finally, impulsive source is replaced by a boat-noise source to show that it is still possible to estimate geoacoustical parameters using noise sources.**

***Index Terms*—Frequency-wavenumber representation, geoacoustical parameters estimation, impulsive and boat sources, propagating modes.**

I. Introduction

In UNDERWATER acoustics, oceanic engineering, and marine geophysics, geoacoustical parameters knowledge (sea-bottom properties, water-layer velocity) is a crucial issue to environmental studies. In underwater acoustics, numerous propagation models have been developed, which are mainly based on the knowledge of the geophysical parameters of the sea and the sea floor. For geotechnical engineers, particularly those in the petroleum industry, these parameters affect the off-shore structure construction. Geophysical parameter knowledge also makes easier earthquake interpretation. As a result, many different methods have been developed depending of the specific experience and needs. Many sea-floor parameters estimations have been proposed by [1]–[3] and in the IEEE JOURNAL OF OCEANIC ENGINEERING on "Inversion techniques and the variability of sound propagation in shallow water" [4], but most have a high computation cost. Estimation made by [5] is based on the Hankel transform: this approach is close to ours, but the subset of estimated parameters is not the same. The techniques described here allow us to estimate a subset of the parameters of a Pekeris guide (water-layer depth, velocities in the water layer and in the seafloor), but with a low computation cost, which are then applied on real data.

As ultralow-frequency (ULF) waves in underwater acoustics (1–100 Hz) are almost non-affected by absorption during their underwater propagation, they propagate at long range and can be used to estimate the geoacoustical parameters even if the source is far from the receivers: this may appear when we will use boat noises as a source. Our objective is to show that, using ULF waves, models of propagation, and appropriate signal-processing tools, extraction of accurate information on the propagation media is possible. At long ranges and for the ULF propagation case, signal transmission is by propagating modes. They must be taken into account during the horizontal propagation between an underwater source and receivers laid on the sea floor. We first study propagating modes to know more about ULF propagation. Then, we use signal-processing tools (frequency-wavenumber representation) and the properties of propagating modes to estimate geoacoustical parameters. Real seismic data, with impulsive source, are used to recover geoacoustical parameters. As real values of these parameters are not exactly known, it is not possible to validate these news methods and we use simulation to do so. A finite-difference algorithm for modeling P(compressional)-SV(shear vertical) wave propagation in heterogeneous media is used. Two cases are studied: the first in an environment similar to the model used in the inversion and the second in a more realistic environment (with several layers of sediments and a variable water-layer depth). Geoacoustical parameters are estimated and compared to the values used in the simulation. In the last part, we present the simulated case of a boat-noise source and show that it is still possible to recover the geoacoustical parameters of the sea and the sea floor.

II. Description of Propagating Modes

A. General Context

Geoacoustical parameters estimation based on wave theory depends on the model of propagation in the acoustic (sea) and elastic (sea-floor) media. The model used here is a range-independent Pekeris waveguide (Fig. 1): a homogeneous fluid layer overlying a homogeneous fluid half-space with no attenuation [6].

Let us consider an omnidirectional impulsive source located under the sea surface (Fig. 2). Waves arriving on the sea floor with an incident angle θ_1 inferior to the critical reflection angle θ_c are partially transmitted in the sea floor. They do not contribute to long-distance propagation (as we will show in Sec-

Manuscript received October 24, 2002; revised April 10, 2003. This work was supported in part by the Délégation Générale pour l'Armement (DGA).

The authors are with the Laboratoire des Images et Signaux, INPG/ENSIEG, Domaine Universitaire, Saint Martin d'Heres, France (e-mail: barbara.nicolas@lis.inpg.fr; jerome.mars@lis.inpg.fr; jean-louis.lacoume@lis.inpg.fr).

Digital Object Identifier 10.1109/JOE.2003.816687

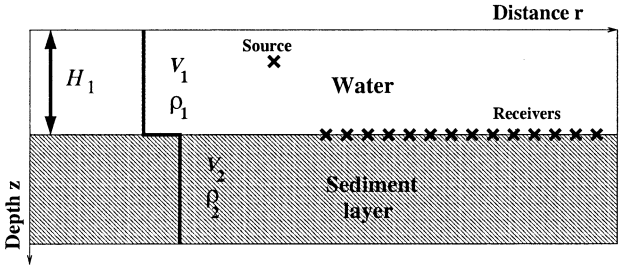

Fig. 1. Model of environment used to estimate geoacoustical parameters.

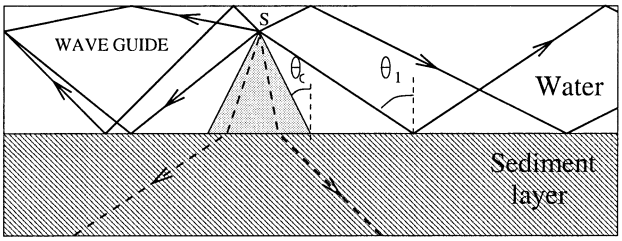

Fig. 2. Propagation approximation.

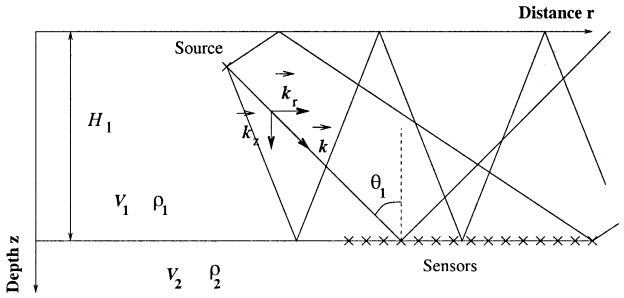

Fig. 3. Waveguide parameters.

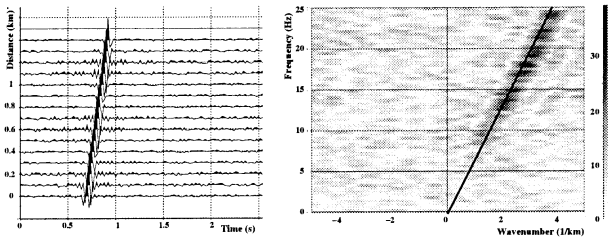

Fig. 4. $r-t$ (left) and $f-k$ (right) representations of a plane wave.

tion II-B), whereas totally reflected waves guided between the sea surface and bottom propagate further in the waveguide. As a result, proposed methods to estimate geoacoustical parameters using ULF waves will be based on wave-guide theory. The experiment is run with one broad-band source in the water column and a horizontal array (with sensors regularly spaced) on the sea floor. Each component of the array records a temporal signal: seismograms, which are two-dimensional (2-D) waveforms with t (time) and r (distance), are generated. We can note that the horizontal array is not necessary and can be replaced by one source moving from one location to another to create synthetic aperture (with only one sensor). This configuration has been used to record real data presented in this paper.

B. Waveguide

A simple model of the Pekeris waveguide is presented on Fig. 3. Parameters necessary for studying the waveguide between an underwater source and receivers laid on the sea floor are: the water depth H_1, the P-wave velocity in the water layer V_1, the P-wave velocity in the first sediment layer V_2, the density of the water layer ρ_1, and the density of the sediment layer ρ_2. R_1 and R_2 are, respectively, the reflection coefficients of the air/water and water/sea-floor interfaces. r represents the distance axis and z the depth axis. $k=(k_r,k_z)$ is the wavenumber[1] and can be projected on distance and depth axis, $k_z=k\cos\theta_1$, $k_r=k\sin\theta_1$ with $k=f/V_1$.

During the propagation path, interferences between different waves (up- or down-going) appear, creating guided waves [6], [7]. The condition of constructive interferences, known as resonance condition, can be written as

$$R_1R_2\exp(4\pi jk_{zm}H_1)=\exp(2\pi jm) \tag{1}$$

[1]By homogeneity with the temporal frequency, k is defined as a spatial frequency. $k=f/V_1$ and is the inverse of the wavelength.

where m is the mode number. If $|R_1R_2|<1$,which is realistic, a part of the energy disappears during the reflection (by transmission to the layer below: leaky guide) and (1) can be written

$$k_{zm}+\frac{\phi_{R_2}}{4\pi H_1}=\frac{2m-1}{4H_1}+j\frac{\log(\|R_2\|)}{4\pi H_1} \tag{2}$$

with $R_1=-1$ and $R_2=\|R_2\|\exp(-j\phi_{R_2})$.

This coefficient R_2 depends on the incident angle θ_1. One particular incident angle is the critical angle θ_c, which is the transmission limit angle. When the incident angle is greater than θ_c, all the incident waves are reflected in the water layer; no energy is transmitted in the sediment layer. For this condition, R_2 simplifies and the relation for the mode m between the frequency f_m and the incident angle θ_1 (or the horizontal wavenumber k_r) is described by

$$\tan\left(\frac{2\pi f_mH_1\cos\theta_1}{V_1}-\left(m-\frac{1}{2}\right)\pi\right)=\frac{\rho_1\sqrt{\sin^2\theta_1-\left(\frac{V_1}{V_2}\right)^2}}{\rho_2\cos\theta_1}. \tag{3}$$

Focusing on the critical angle $\theta_1=\theta_c$, (3) simplifies and allows us to recover the cutoff frequency of each mode [8], [9]

$$f_{cm}=\frac{(2m-1)V_1}{4H_1\sqrt{1-\left(\frac{V_1}{V_2}\right)^2}}. \tag{4}$$

C. Measuring the Mode Cutoff Frequencies Using $f-k$ Transform

1) Characterization of the Modes in the Distance-Frequency Domain: The pressure field in space (r,z) and frequency (f) can be expressed as a sum of modes [8], [9] as

$$P(r,z,f)=S(f)\sum_m A_m(f)\Psi_m(f,z)X_m(f,r) \tag{5}$$

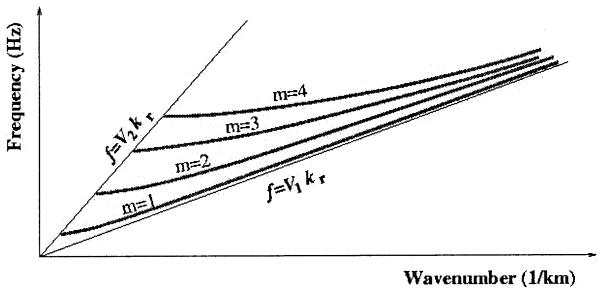

Fig. 5. Modes representation in the $f-k$ domain.

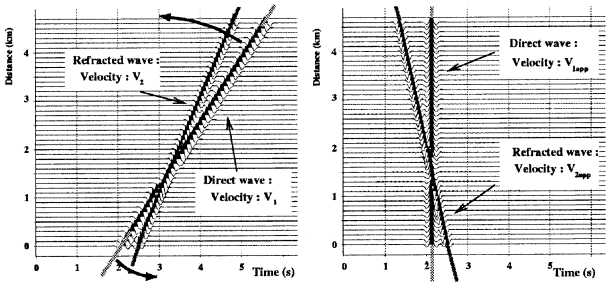

Fig. 6. Synthetic time-distance section before (left) and after (right) velocity V_1 correction.

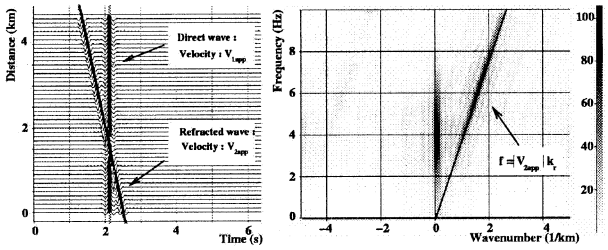

Fig. 7. $r-t$ (left) and $f-k$ (right) representations of the direct and refracted waves.

with $A_m(f)$, excitation factor of the mode m; $\Psi_m(f,z)$, energy repartition along the depth axis z; and $X_m(f,r)(1/\sqrt{r})\exp(-2\pi j k_{rm}(f)r)$, radial propagation.

The propagating waves for long-range signal transmission are those arriving on the sea floor with an incident angle inferior to the critical angle. Indeed, if $\theta_1 < \theta_c$, k_{rm} has an imaginary part (2) that induces absorption in $X_m(r)$, which is not the case if $\theta_1 > \theta_c$ (k_{rm} is real). As a result, the approximation made in Section II-A, which consists in taking into account only waves arriving with an incident angle greater than the critical angle, is justified.

2) Frequency-Wavenumber Transform: In order to characterize propagating modes, we introduce the "frequency-wavenumber" representation, which is the square modulus of the 2-D Fourier transform of a section $p(r,z,t)$ in time t and radial distance r at a given depth z [10]. This representation, named $f-k$ representation, is

$$P(k_r,z,f)=\int\int p(r,z,t)\exp(-2\pi j(ft-k_r r))dtdr. \quad (6)$$

The origins of time and distance do not affect the $f-k$ representation as we take the modulus of the 2-D Fourier transform: indeed, when the distance origin changes, $\exp(-2\pi j r_0)$ appears in the 2-D Fourier transform, but its modulus is equal to 1.

We can illustrate the $f-k$ transform as a plane wave with velocity V becoming a straight line of slope V in the frequency-wavenumber domain: $f=Vk_r$. Fig. 4 shows a plane wave and its $f-k$ representation.

3) Propagating Modes Characterization in Frequency-Wavenumber Domain: At depth z_0, the pressure field becomes

$$p(k_r,z_0,f)\approx S(f)\sum_{m=1}^{\infty}A_m(f)\Psi_m(f,z_0)\delta[k_r-k_{rm}]. \quad (7)$$

This expression shows that pressure only depends on the source spectrum. As a result, all the processing in the frequency-wavenumber domain $(f-k)$ will still be efficient when the explosive source will be replaced by a boat source in detection problems (as long as this source has a broad-band spectrum). The $f-k$ representation (Fig. 5) permits the separation of the different modes [6], [8]: if the incident angle is inferior to the critical angle, waves do not propagate at long range. As a result, the limit waves that can interfere in the waveguide have a wavenumber oriented in the critical angle direction. In this case, $k_z=f\cos\theta_1/V_1$ becomes

$$k_z=\frac{f}{V_1}\sqrt{1-\left(\frac{V_1}{V_2}\right)^2}. \quad (8)$$

Using $k_{rm}^2+k_{zm}^2=f/V_1$, we obtain $k_{rm}=f/V_2$, which is a straight line passing through the cutoff frequencies. The other limit-of-incident angle is when the wavenumber is oriented in the horizontal direction $(k_{zm}=0)$. In this case, $k_{rm}=f/V_1$ is the asymptote above which modes exist in the $f-k$ domain [11]. Between these two straight lines, modes propagate and verify (3). This relation, expressed with respect to the horizontal wavenumber k_r, represents the modes in the $f-k$ domain.

III. Geoacoustical Parameters Estimation

In this section, signal-processing tools are used to estimate geoacoustical parameters of water-layer velocity V_1, first sedimentary-layer velocity V_2, and water depth H_1 [10], [12], [13].

A. Estimation of the Water-Layer Velocity V_1

Propagation in the water layer is first characterized by a direct wave recorded on receivers laid on the floor. Temporal positions of the arrivals depend on the offset between the underwater source and each receiver. To estimate V_1, from initial section in the distance–time domain $[r,t]$, we apply a time correction along the distance axis r. The recorded signal of each sensor is time shifted so that the direct wave impinges on all sensors at the same time. This time correction gives an estimation of the water-layer velocity V_1. Fig. 6 shows an example of V_1 velocity correction on a simple seismic section.

B. Estimation of the Velocity V_2 in the First Sediment Layer

Refracted waves propagate in the water column and then at the water/sea-floor interface. Their velocity is the sedimentary medium velocity. So, to estimate V_2, classical techniques [13] are based on the refracted wave identification and on its velocity estimation. A small part of the seismic section recorded on the sensors is extracted. This section is chosen so that direct and refracted waves can be identified, then estimation is possible on

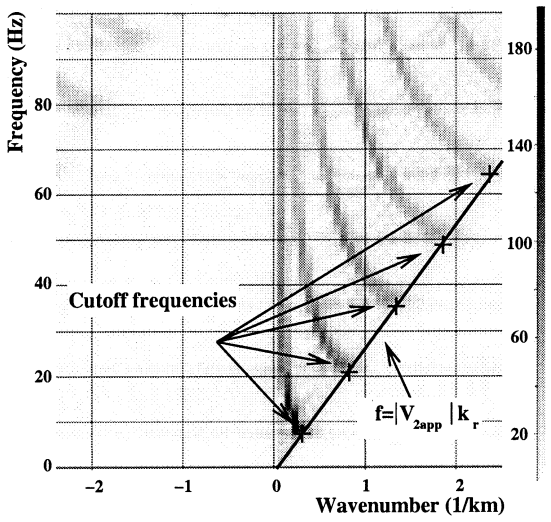

Fig. 8. $f-k$ representation of the pressure seismogram.

the $f-k$ representation. After the correction of the water-layer velocity V_1 [Fig. 7 (left)], the refracted wave velocity V_2 is given by

$$V_2 = \left[\frac{1}{V_{2\text{app}}} + \frac{1}{V_1}\right]^{-1} \tag{9}$$

where $V_{2\text{app}}$ is the apparent refracted wave velocity measured on the $f-k$ representation [Fig. 7 (right)]. This estimation is possible only if sensors are quite close to the source. With sensors far from the source, refracted waves cannot be seen due to their large attenuation at long distance.

To avoid this problem, we prefer using $f-k$ representation of the seismic section recorded on the sensors, which are at long range (Fig. 8). We only take sensors at long range as we assume plane waves. This $f-k$ representation shows different modes of propagation and allows us to use physical characterization established in the first part of this paper. After V_1 velocity correction, the asymptote $f = V_2 k_r$ is shifted in $f = V_{2\text{app}} k_r$ (with $V_{2\text{app}}$ defined above). As a result, we can find V_2 by estimating the slope of this straight line after the V_1 velocity correction.

C. Estimation of the Water Depth H_1

Water depth is measured directly on the $f-k$ plot (Fig. 8). All cutoff frequencies are extracted in terms of temporal frequency coordinates. Knowing V_1 and V_2, (4) allows us to recover the water depth H_1.

IV. Applications on Real and Simulated Data With Impulsive Source

Our objective is to extract geoacoustical parameters from a real data set generated by an impulsive source. We first apply methods described above on this data set. As real values of these geoacoustical parameters are not exactly known, it is not possible to validate the methods described in the first part with this data set. Then, a finite-difference algorithm for modeling P(compressional)-SV(shear vertical) wave propagation in heterogeneous media is used. Two cases are studied: the first in an environment similar to the model used in the inversion and the second in a more realistic environment (with several layers of sediments and a variable water-layer depth). Geoacoustical parameters are estimated and compared to the values used in the simulation.

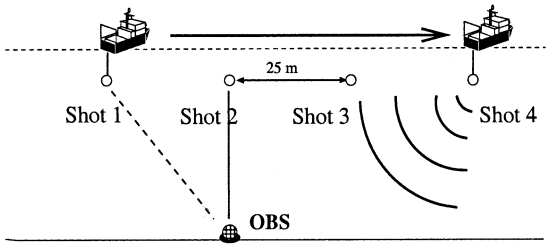

Fig. 9. Geometry of the experiment.

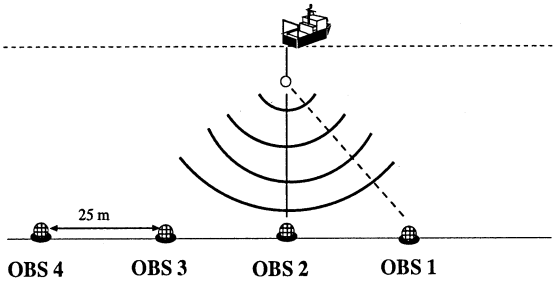

Fig. 10. Equivalent geometry: synthetic aperture created by the displacement of the source.

A. Application on Real Data

Techniques described above are now used on real data to recover geoacoustical parameters. The experimental geometry is shown in Fig. 9. The source is an air gun moving from one location to another, making one shot every 25 m. The receiver is a four-component ocean-bottom seismometers (OBS), which provides the three components of the displacement and the pressure field. As a result, field data set is recorded on a synthetic antenna of 240 OBS laid on the North Sea floor. This geometry creates synthetic aperture and is equivalent to that presented in Fig. 10, which allows us to use methods described above. In this application, the hydrophone is mainly used, but vertical geophone gives identical results for our objective. Spatial and time sampling are, respectively, 25 m and 4 ms [12]. Initial data are time corrected with velocity $V_1 = 1520\,\mathrm{m/s}$, as explained in the synthetic data in Section III-A. Results in the time-distance domain and temporal frequency-spatial frequency domain are presented in Figs. 11 and 12.

We first focus on a small part of the entire section to determine V_2, thanks to the refracted head wave. This window (Fig. 13), extracted from the pressure seismogram (Fig. 11) in the distance-time domain, is centered around the origin of the time and distance axis. It is chosen so that identifications of the direct and refracted waves could be made. A $f-k$ transform of the extracted section is computed and the estimation of V_2 is, using the expression between V_2 and V_{2app}, $V_2 = 1906\,\mathrm{m/s}$.

The other possibility to estimate V_2, which consists of using modes, is also used (Fig. 12). $f-k$ transform of the seismic section (Fig. 11) from 2 to 6 km allows us to find the slope of the straight line passing through the cutoff frequencies and so

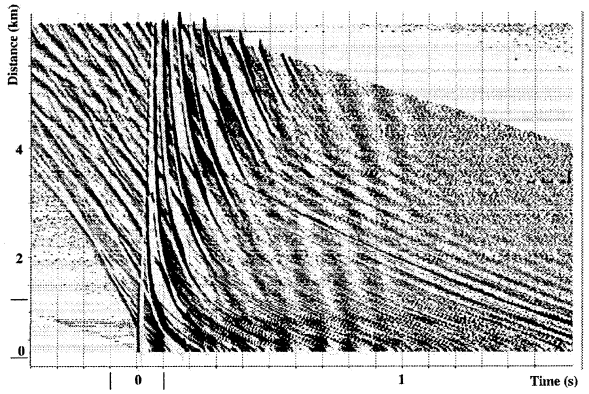

Fig. 11. Pressure seismogram section after V_1 velocity correction.

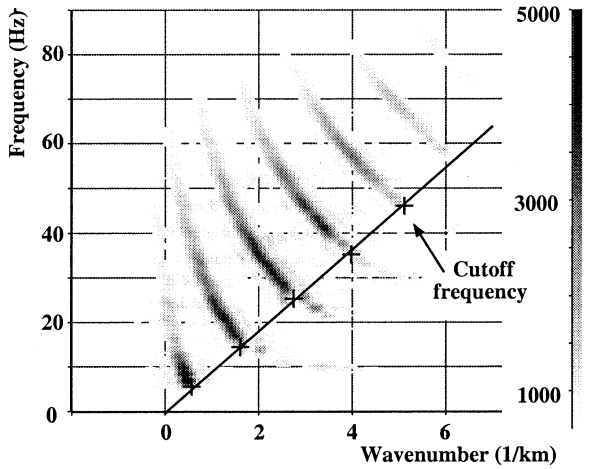

Fig. 12. $f-k$ transform of the real data section of Fig. 11 from 2 to 6 km.

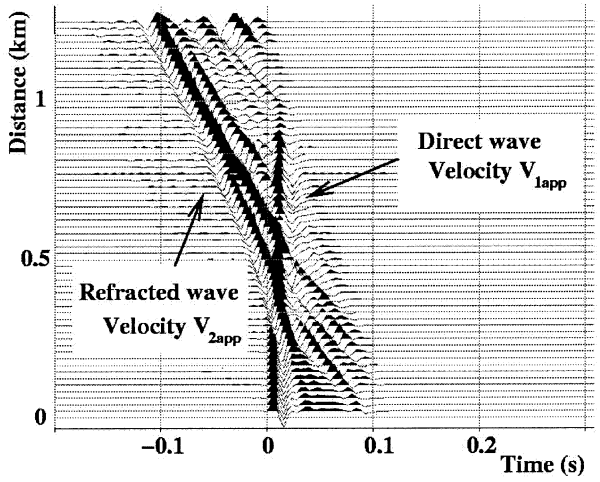

Fig. 13. Direct and refracted waves extracted from 11.

TABLE I
ESTIMATION OF WATER DEPTH

Modes	1	2	3	4	5
Freq(Hz)	6.9	14.7	25.0	35.4	45.0
Depth(m)	94.1	132.4	129.8	128.3	129.8

to determine $V_2 = 1876$ m/s. Results are close: estimations only differ from 1.6% from one method to the other. Then H_1 is estimated with (4). Cutoff frequencies of the different modes give several values for H_1 (Table I).

We remove estimation of H_1 given by the first mode because estimation of f_{c1} is known with an uncertainty of 1 Hz, which represents a relative uncertainty of 20% (f_{c1} is around 5 Hz). The estimated value of H_1 is then $H_1 = 130.1$ m.

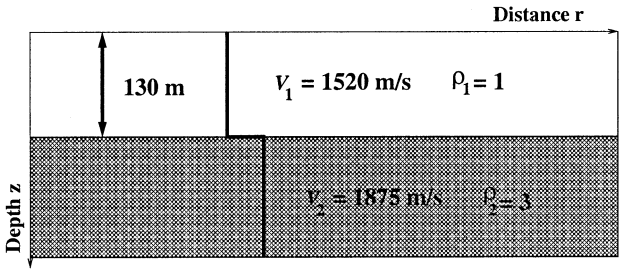

Fig. 14. Environment used to simulate a Pekeris waveguide.

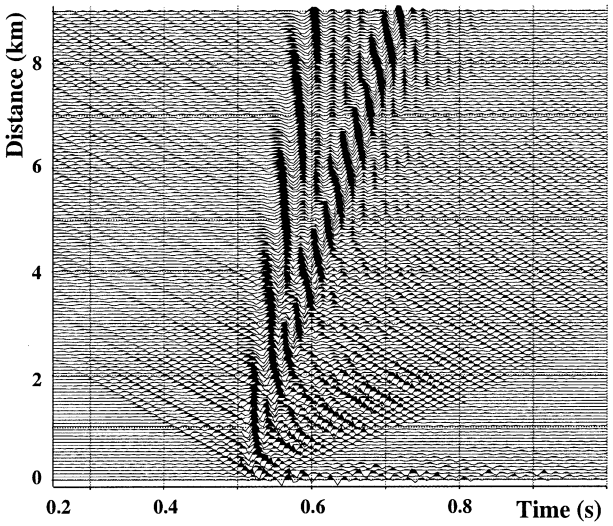

Fig. 15. Pressure seismogram section after V_1 velocity correction.

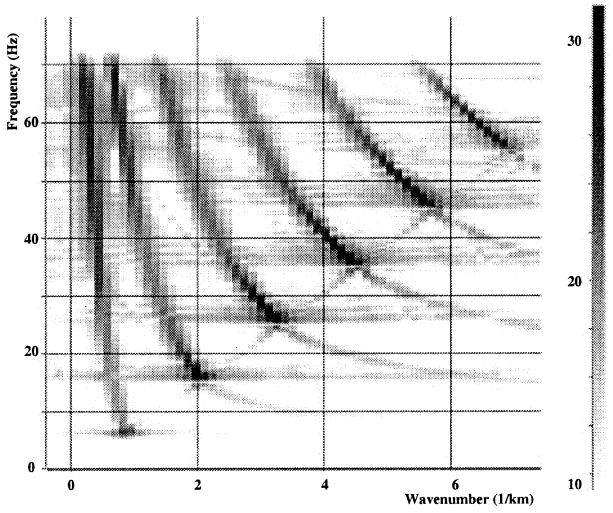

Fig. 16. $f-k$ transform of the simulated section of Fig. 15 between 2–8 km in range.

B. Application on Simulated Data

To validate methods presented in Section III, geoacoustical parameters are estimated on data simulated by a finite-difference method for modeling propagation of P and SV waves in heterogeneous media. This time-distance algorithm, computed by Virieux [14], gives stable results for step velocity discontinuities, which is the case for a water layer above an elastic media.

We first simulate data in an environment similar to Pekeris guide and with parameters estimated in Section IV-A. The model is presented in Fig. 14 and uses the previous estimated geoacoustical parameters $V_{1_0} = 1520\ \mathrm{m/s}$, $V_{2_0} = 1875\ \mathrm{m/s}$, $H_{1_0} = 130\ \mathrm{m}$. An explosive source is simulated by an impulsive function (sinc) with a bandwidth of 0–80 Hz and the data are sampled at intervals of 5 ms. The source and receivers depths are, respectively, 20 and 130 m. 200 OBS at intervals of 60 m are used to record the pressure field and the displacements. Our objective is to recover these simulated geoacoustical parameters using previous methods on the simulated data set and to compare results. Figs. 15 and 16 present the time-distance and frequency-wavenumber plots of the simulated data set.

After processing, estimation of V_1 is 1520 m/s. The second parameter that we estimate is the velocity of the second layer. This layer is often a sedimentary layer saturated with water. Two methods (refracted wave identification and $f-k$ asymptote characterization) are used to determine V_2:

- refracted waves velocity: $V_2 = 1884\ \mathrm{m/s}$;
- asymptote in the $f-k$ domain (Fig. 16: $f-k$ transform of the pressure seismogram between 2 to 8 km in range): $V_2 = 1880\ \mathrm{m/s}$.

We observe that these two velocities are close. In practice, the second estimation is closer to the reality and easier to perform than the first one. Finally, cutoff frequencies given by studying the $f-k$ representation allow an estimation of H_1 (Table II).

As was done on real data, an average water depth is calculated: $H_1 = 128.1\ \mathrm{m}$. We can compare estimated values to values used to simulate

$$V_1 = V_{1_0} + 0\% \tag{10}$$
$$V_2 = V_{2_0} + 0.5\% \tag{11}$$
$$H_1 = H_{1_0} + 1.4\%. \tag{12}$$

To conclude, methods proposed in Section III seem to be efficient to estimate geoacoustical parameters when the environment is similar to a Pekeris waveguide. As is not the case with real data, it can be interesting to see what happens when the media differs from these assumptions.

Another simulation is performed in the environment described on Fig. 17. The subsurface is made of two sediments layers and the water depth varies from 126 to 132 m. Source and receivers are the same as in the previous simulation. Using Fig. 18 and methods described in Section III, we obtain $V_1 = 1520\ \mathrm{m/s}$, $V_2 = 1894\ \mathrm{m/s}$, and $H_1 = 129.0\ \mathrm{m}$.

We can compare estimated values to values used to simulate

$$V_1 = V_{1_0} + 0\% \tag{13}$$
$$V_2 = V_{2_0} + 1.0\% \tag{14}$$
$$H_1 = H_{1_0} + 0.7\%. \tag{15}$$

TABLE II
ESTIMATION OF WATER DEPTH

Modes	1	2	3	4	5
Freq(Hz)	5.5	15.3	25.3	35.6	45.1
Depth(m)	118.0	127.2	128.3	127.6	129.5

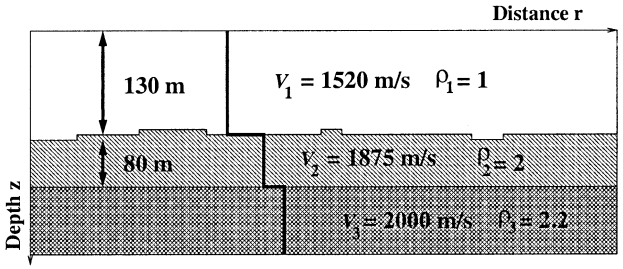

Fig. 17. Environment used in the second simulation: a realistic environment with several layers in the subsurface and a water depth varying from 126 to 132 m.

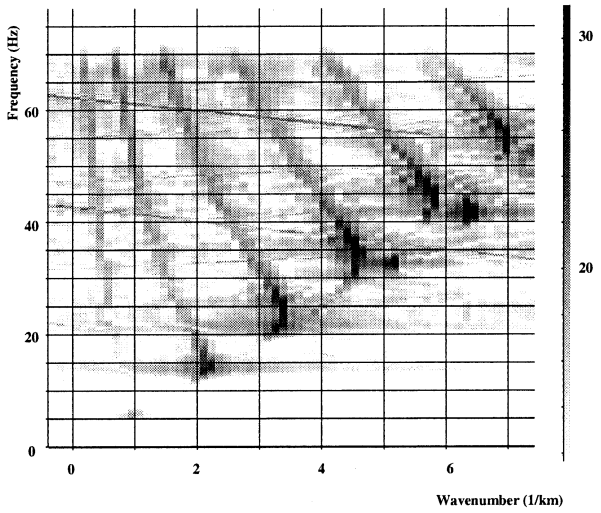

Fig. 18. $f-k$ transform of the simulated section with a realistic environment (sensors between 2–8 km in range).

As a result, methods proposed to estimate geoacoustical parameters are still efficient when the environment differs from the simple model of a Pekeris waveguide. The next step is to try these methods on data with a boat source.

V. APPLICATION ON SIMULATED DATA WITH A BOAT-NOISE SOURCE

Techniques presented in Section III are applied to synthetic data to demonstrate the usefulness of the method in estimating the geoacoustical properties of the water and topmost sediment layers in the case of a boat-noise source. The source is a boat noise and time sampling is 2.5 ms. The source lasts 5 s and its spectrum is located in the 1–100 Hz band. The duration of the source is quite short: it is due to the simulation algorithm, which is long to perform in these conditions, but in the frequency-wavenumber domain the results would be kept with a longer source. A temporal representation of the source and its spectrum are respectively, shown on Figs. 19 and 20. The main difference between the explosive source and the boat-noise

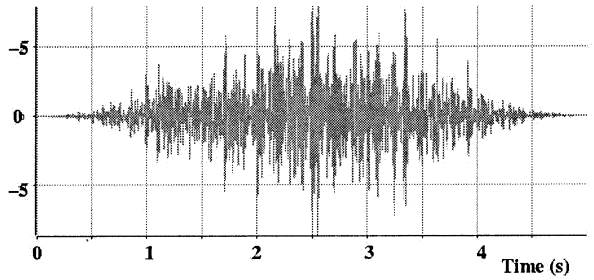

Fig. 19. Source: recording of a boat noise.

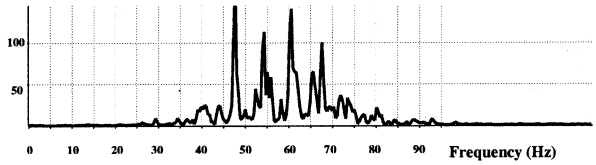

Fig. 20. Spectrum of the source.

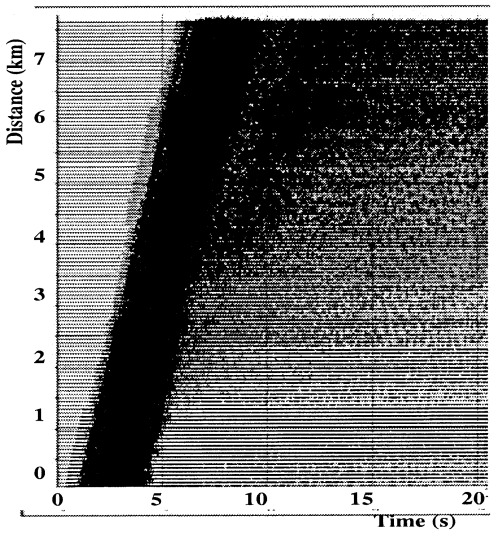

Fig. 21. Vertical-displacement seismogram.

source is that the spectrum of the first is flat, whereas the other presents many peaks. The other parameters of the simulation are the same as those in Section IV-B. A finite-difference algorithm is used to simulate the propagation and we try to recover the geoacoustical parameters.

Synthetic seismogram (Fig. 21) of the vertical component of the displacement field is calculated. It is impossible to recover the geoacoustical parameters on the time-distance representation (such as using the refracted wave velocity to estimate V_2). As is the case for the pressure field, the displacement can be written as a sum of modes with the source spectrum in factor. As the source spectrum is not flat, the $f-k$ representation (Fig. 22) of the vertical-displacement seismogram is the product of the $f-k$ representation obtained with the explosive source and that of the ship-source spectrum. It is still possible to identify the different modes, but it becomes harder when the source spectrum presents a peak (55 Hz) or a valley (50 Hz). A blind whitening [15] can be used (Fig. 23) to flatten the spectrum and the $f-k$ representation of the vertical displacement allows us to recover the geoacoustical parameters.

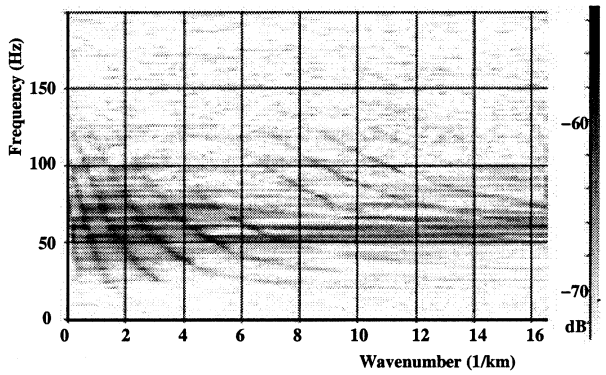

Fig. 22. $f-k$ transform of the simulated section in Fig. 21 without whitening.

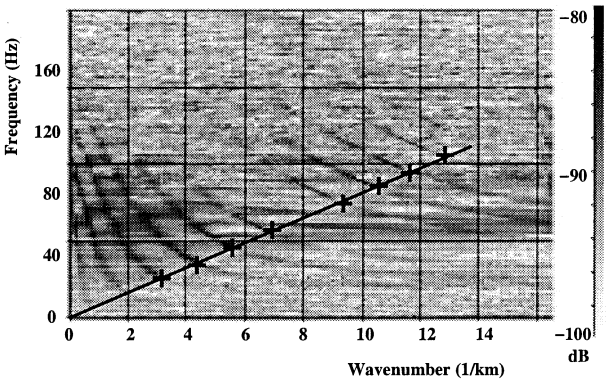

Fig. 23. $f-k$ transform of the simulated section in Fig. 21 after whitening.

After velocity correction, V_1 is measured at 1515 m/s. The velocity of the first sediment layer V_2 is estimated using the slope of the straight line passing through the cutoff frequencies $V_2 = 1859\ \mathrm{m/s}$. The water depth is recovered using (4) and the cutoff frequencies measured on the $f-k$ representation $H_1 = 127.5\ \mathrm{m}$. We can compare estimated values to values to be used in the simulation as

$$V_1 = V_{1_0} + 0.3\% \tag{16}$$

$$V_2 = V_{2_0} + 0.8\% \tag{17}$$

$$H_1 = H_{1_0} + 1.9\%. \tag{18}$$

To conclude, methods to estimate geoacoustical parameters are still efficient when the explosive source is replaced by a boat-noise source, as long as the source has a broad-band spectrum. It can be very useful for localization: first, the media of propagation is identified and then the appropriate algorithm of localization can be used to estimate the source position. The last step would be to apply the methods to real ship-noise data.

VI. Conclusion

Underwater sources produce low-frequency signals (<100 Hz) that propagate at long range. In this frequency domain and in shallow-water configuration, wave propagation is mainly described by propagating modes. This type of propagation is well studied in marine geophysics. We have illustrated here that specific methods can be developed to estimate geoacoustical parameters using ULF waves. Propagating modes have been briefly presented to explain propagation and

information carried by these waves. Different transformations (frequency-wavenumber transformation, velocity correction) have been applied to estimate geoacoustical parameters on a real data set with an explosive source. To validate our results, simulated data obtained by a finite-difference algorithm for modeling wave propagation in heterogeneous media has been studied. Finally, we used simulated surface-ship data to demonstrate that the inversion method presented in this paper would also work with sources of opportunity, such as surface ships, as long as they exhibit a broad-band spectrum. The next step would consist of localizing sources using these parameters.

ACKNOWLEDGMENT

The authors thank CGG and DGA for providing real data set, D. Fattaccioli and J. R. Hartman for helpful discussions, J. Virieux and Dr. S. Operto for providing the modeling software, and the reviewers for their interesting remarks.

REFERENCES

[1] N. R. Chapman and C. E. Lindsay, "Matched-field inversion for geoacoustic model parameters in shallow water," *IEEE J. Oceanic Eng.*, vol. 21, pp. 347–354, Oct. 1996.

[2] L. Amudsen and A. Reitan, "Estimation of sea-floor wave velocities and density from pressure and particle velocity by AVO analysis," *Geophys.*, vol. 60, pp. 1575–1578, 1995.

[3] G. V. Frisk and J. F. Lynch, "Shallow water waveguide characterization using the Hankel transform," *J. Acoust. Soc. Amer.*, vol. 76, pp. 205–216, 1984.

[4] *IEEE J. Oceanic Eng.*, vol. 21, 1996. Inversion techniques and the variability of sound propagation in shallow water.

[5] G. R. Potty, J. H. Miller, J. F. Lynch, and K. B. Smith, "Tomographic inversion for sediment parameters in shallow water," *J. Acoust. Soc. Amer.*, vol. 108, pp. 973–986, 2000.

[6] C. L. Pekeris, "Theory of propagation of explosive sound in shallow water," *Geol. Soc. Amer. Mem.*, vol. 27, 1948.

[7] C. S. Clay and H. Medwin, *Acoustical Oceanography: Principles and Applications*. New York: Wiley, 1977.

[8] F. B. Jensen, W. A. Kupperman, M. B. Porter, and H. Schmidt, *Computational Ocean Acoustics*. New York: AIP Press, 1994.

[9] L. M. Brekhovskikh and Y. P. Lysanov, *Fundamentals of Ocean Acoustics*. Berlin, Germany: Springer-Verlag, 1991.

[10] M. Nardin, F. Glangeaud, and D. Mauuary, "1–200 Hz wave propagation in shallow water," in *Proc. IEEE/MTS Oceans'98*, Nice, France, 1998.

[11] I. Tolstoy and C. S. Clay, *Ocean Acoustics*.

[12] X. Dagany, J. Mars, and F. Luc, "Multicomponent data analysis and wave separation in marine seismic survey," in *Proc. 63rd Meet. Eur. Assoc. Geoscientists Engineers, Expanded Abstract*, Amsterdam, The Netherlands, 2001.

[13] F. Glangeaud, J.-L. Mari, J.-L. Lacoume, J. Mars, and M. Nardin, "Dispersive seismic waves in geophysics," *Eur. J. Env. Eng. Geophysics*, vol. 3, pp. 265–306, 1999.

[14] J. Virieux, "P-SV wave propagation in heterogeneous media: velocity-stress finite-difference method," *Geophys.*, vol. 51, pp. 889–901, 1986.

[15] J. Max and J.-L. Lacoume, *Méthodes et Techniques de Traitement du Signal*. Paris, France: Dunod, 2000.

Barbara Nicolas graduated from the Electrician Engineers National Superior School of Grenoble, Grenoble, France, in 2001 and received the Diplome d'Etudes Approfondies (DEA) in signal image and speech from the National Polytechnic Institute of Grenoble, France, in 2001. She is currently working toward the Ph.D. degree at the Laboratoire des Images et Signaux, Grenoble, France. Her work is supported by the Délégation Générale pour l'Armement (DGA).

Her research interests include geoacoustical parameters estimation and characterization of ultralow-frequency waves for localization.

Jérome Mars received the M.S. degree in 1986 in geophysics from Joseph Fourier University of Grenoble, Grenoble, France, and the Ph.D. degree in signal processing in 1988 from the Institut National Polytechnique of Grenoble, Grenoble, France.

From 1989 to 1992, he was a Postdoctoral Researcher at the Centre des Phénomènes Aléatoires et Geophysiques, Grenoble, France. From 1992 to 1995, he was a Visiting Lecturer and Scientist in the Materials Sciences and Mineral Engineering Department, University of California, Berkeley. He is currently an Assistant Professor of Signal Processing at the Institut National Polytechnique de Grenoble and is with the Laboratoire des Images et Signaux, Grenoble, France. His research interests include seismic and acoustic signal processing, wavefield separation methods, time-frequency time-scale characterization, and applied geophysics.

He is a member of Society of Exploration Geophysicists (SEG) and European Association of Geoscientists and Engineers (EAGE).

Jean-Louis Lacoume (SM'92) was born in Mirepoix, France, on November 30, 1940. He graduated from the Ecole Normale Supérieure, Paris, France, as a certified teacher in 1964 and Docteur d'état in 1969.

He was a Lecturer in physics at Orsay University, Orsay, France, from 1964 to 1967) and in geophysics at Paris VI University from 1969 to 1972. He has been a Professor at the National Polytechnic Institute of Grenoble (INPG), Grenoble, France, since 1972, where he studies waves physics and signal processing. He has published seven books and 50 papers on reviews and 110 communications on conferences. His research and teaching activities are in wave physics and signal processing; electromagnetic waves in the earth environment; acoustic and elastic waves in the earth and the oceans; vibrations of mechanical systems; spectral and cross-spectral analysis; and higher order statistics.

Dr. Lacoume was Director of the Research Center on Random Phenomena and Geophysics (CEPHAG), Grenoble, France, from 1972 to 1989, Dean of the Post-Graduate School at INPG from 1989 to 1995, and Director of the Laboratoire des Images et Signaux (LIS), Grenoble, France, from 1998 to 2000.